Hindawi
Shock and Vibration
Volume 2024, Article ID 6686238, 12 pages
https://doi.org/10.1155/2024/6686238

Research Article

A Multifactor Combination Optimization Design Based on Orthogonality for a Two-Degree-of-Freedom Floating Machine Gun Vibration System

Yang Wang[1], **Cheng Xu**[1], **Long He**[1] and **Yanfeng Cao**[1,2]

[1]*School of Mechanical Engineering, Nanjing University of Science and Technology, Nanjing 210094, China*
[2]*Science and Technology on Transient Impact Laboratory, Beijing 102202, China*

Correspondence should be addressed to Cheng Xu; xucheng62@njust.edu.cn

Received 25 July 2023; Revised 19 February 2024; Accepted 2 March 2024; Published 11 March 2024

Academic Editor: Bao-Jun Shi

This paper introduces a novel type of floating machine gun that can be simplified as a self-balancing two-degree-of-freedom mechanical system with distinct vibration characteristics. The model accounts for intricate motion patterns and encompasses numerous potential influencing factors. Multifactor combination optimization of the system represents a pressing engineering challenge. After establishing a simulation model for the machine gun and validating it experimentally, seven factors were chosen as optimization variables. The maximum recoil displacement of the inner receiver (MRD) and the firing rate were chosen to be indicators. Orthogonal combinations and variance analyses were used, and the effects of multiple factors were analyzed using SPSS software; these processes led to a determination of the optimal combination. The results indicated that the piston cylinder pressure, the bi-directional buffer spring energy storage, and the inner receiver mass significantly affected the MRD. Furthermore, the automaton mass and the reset spring energy storage were found to substantially affect the firing rate. Careful analysis of the variance results facilitated the determination of the optimal combination of parameter values. Remarkably, the optimal combination chosen resulted in an MRD reduction of approximately 20.2% and a firing rate increase of approximately 26.6%.

1. Introduction

The floating principle is an innovative design approach used for firearms. It is predominantly applied to open-bolt machine guns and small-caliber cannons. A traditional firearm can be simplified as a single-degree-of-freedom system, in which an automaton moves back and forth inside the receiver and generates impacts. These impacts are ultimately transmitted to the firearm tripod or a human body, thereby causing the firearm to vibrate along with the tripod or body. In contrast, a floating firearm possesses an additional inner receiver between the automaton and the receiver, and it is therefore a two-degree-of-freedom system. The impacts from the automaton are transmitted to the inner receiver. Then the vibrations that would normally be transmitted to a tripod or a human body are largely transformed into vibrations of the inner receiver. As a result, the tripod or human body vibrations are significantly reduced, which is beneficial for increasing the shooting accuracy and stability of the firearm. Notably, several types of firearms, such as the General Dynamics Lightweight Medium Machine Gun, the SIG Arms MG338 machine gun, and the new XM250 machine gun developed for the Next Generation Squad Weapons program by the US Army, have adopted the floating principle [1–3].

During the firing process of a floating firearm, the inner receiver vibrates between extreme recoil and return points without colliding with the receiver [4]; this is how the firearm earns its "floating" designation. During the mechanical design of a floating firearm, the floating (or vibration) amplitude should be kept as small as possible. In practical applications, since the recoil energy of a firearm is significantly greater than its return energy, the extreme return displacement is often more than sufficient in application.

Consequently, the primary assessment criterion used for achieving ideal floating is the maximum recoil displacement (MRD) of the inner receiver. Ideally, the MRD should be minimized [5]. In addition, for firearms utilizing the floating principle, the vibration frequency of the entire two-degree-of-freedom system, or the firing rate, tends to be low; thus, it is necessary to increase the firing rate. Therefore, the MRD and the firing rate are crucial design considerations for two-degree-of-freedom floating firearm systems.

Currently, research regarding floating firearms predominantly utilizes a methodology that involves modifying specific input parameters to investigate the effects of parameter variations on the results. For example, Lu et al. studied the effects of muzzle brakes and piston parameters on floating firearms [6–9]. However, though muzzle brakes and piston parameters are factors that commonly influence traditional machine guns, floating firearms may be influenced by many unique parameters that have not yet been addressed. Wang investigated the effects of the floating lock position [10], which is a specific factor of floating technology. However, this study only focused on examining the impacts of this single factor. Additionally, the floating lock is a mechanism typically used in earlier floating technology, while the new floating mechanism described in this paper does not possess a floating lock. In addition, Yongjian et al. explored the use of floating technology in modified rifles for unmanned aerial vehicles [11] while studying recoil reduction in floating firearms. None of the abovementioned studies addressed multifactor optimization of floating machine guns.

Floating machine guns are two-degree-of-freedom systems and thus introduce novel and distinct influencing parameters that interact in intricate ways, thereby yielding complex relationships. As a result, the research methods mentioned earlier are not equipped for analyzing two-degree-of-freedom systems. Using the MRD and firing rate as examples, a multifactor analysis method was employed during the current study to examine the effects of various parameters on a firearm floating mechanism. The study identified the optimal combination of parameters that would enhance the floating performance of the firearm.

This paper contains three innovative aspects. First, it introduces a new type of floating machine gun model. In the floating machine gun industry, this model represents an entirely new technology. Second, new technologies inevitably bring new potential influencing factors. The impacts of these factors on the floating mechanism were explored during this study, and this exploration encompassed an area not addressed in previous research. Finally, the paper presents joint optimization results involving multiple factors. These kinds of results also remained unexplored during prior research.

2. Simulation Model of the Two-Degree-of-Freedom Floating Machine Gun

2.1. Simulation Model of the Floating Machine Gun. The core mechanism of a traditional machine gun can be simplified as a single-degree-of-freedom model, as shown in Figure 1(a). The automaton moves back and forth within the receiver, and when it reaches the left end or the right end of the receiver, it violently impacts the receiver. Figure 1(b) shows that, in the floating machine gun described in this paper, there is an additional inner receiver between the automaton and the receiver. The inner receiver is connected to the automaton by a reset spring, while it is connected to the receiver by a bi-directional buffer spring. In a traditional machine gun, when the automaton reaches its rearmost or foremost position, it impacts the receiver and transmits the impact to the human shooter or the gun mount. In the floating machine gun described in this paper, however, the impacts are transmitted to the inner receiver and are absorbed by the bi-directional buffer spring.

The marked points on the receiver in Figure 1(b) are denoted as O_1, O_2, and O_3, while those on the inner receiver are denoted as O_4, O_5, and O_6. O_2 and O_5 represent the points of zero displacement of the automaton and the inner receiver, respectively, while O_1 and O_3 represent the extreme recoil and extreme return points, respectively, of the inner receiver. Figure 2 depicts the correlation between the extreme recoil and extreme return points, as well as the corresponding displacements, namely, the extreme recoil and extreme return displacements. Figure 2 also illustrates their relationships with the MRD.

The floating machine gun model presented in this paper is similar to the car tire-ground model, which is one of the most common two-degree-of-freedom models [12]. Car models are subject to random vibrations from the ground, while the external forces on the floating machine gun are triggered when the automaton moves to a certain location. Car models must pursue smaller human body or vehicle body vibration amplitudes to ensure comfort, while machine gun models must pursue smaller inner receiver vibration amplitude.

In this paper, motion in the recoil direction, such as that which occurs when the automaton travels from O_6 to O_4, is defined as positive, while motion in the opposite direction, which is defined as the return direction, is defined as negative. Figure 3 illustrates the internal ballistic force and the piston cylinder force on the inner receiver, the piston cylinder force on the automaton, and the feeding resistance using purple, blue, green, and yellow arrows, respectively. It is important to note that the piston cylinder forces acting on the inner receiver and the automaton have equal magnitudes but opposite directions.

Figure 3(a) shows that when the automaton return motion is initiated by the reset spring, resistance is imposed by the feeding mechanism. In Figure 3(b), the automaton has just reached position O_6 and has thus collided with the inner receiver. Figure 3(c) illustrates that this collision impels the inner receiver, which is positioned at O_2, to commence the return motion by firing a bullet.

Because the internal ballistic force has a greater magnitude than the piston cylinder force, the inner receiver recoils under the combined effect of both forces. In contrast, the automaton recoil is solely attributable to the piston cylinder force. Figure 3(d) indicates that the reset spring causes the automaton to decelerate and that the inner

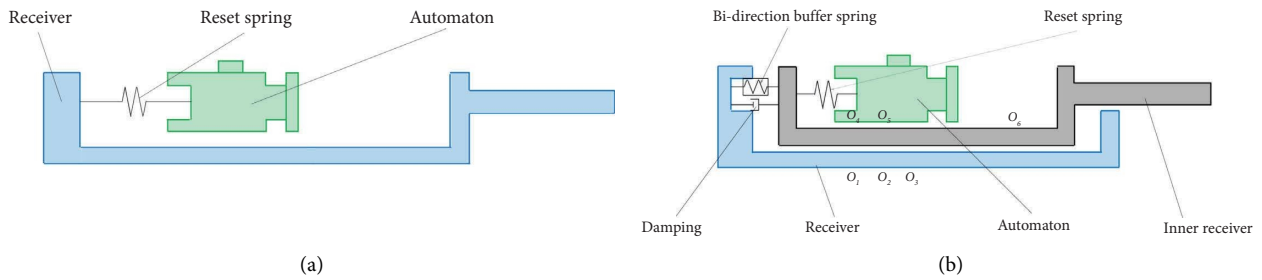

Figure 1: Schematic of the two-degree-of-freedom floating machine gun.

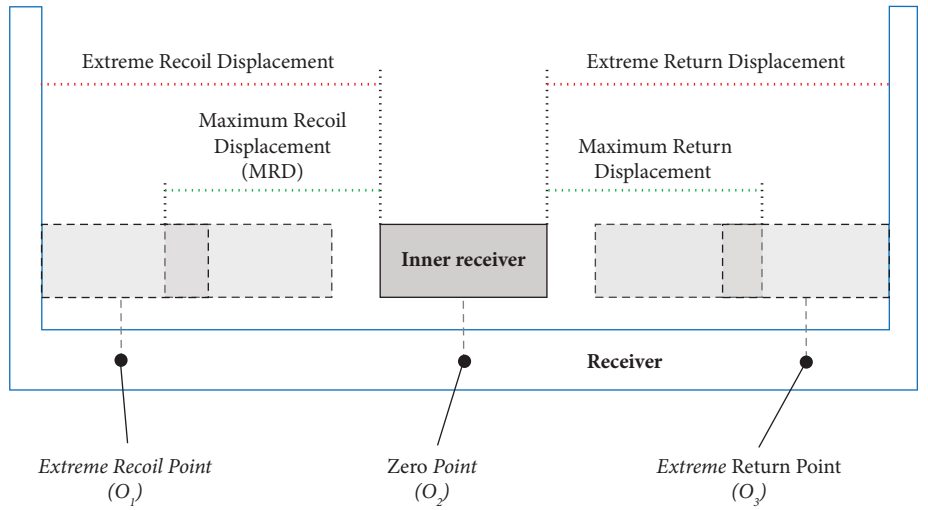

Figure 2: Positional relationships between the extreme recoil point, the extreme return point, the displacements, and the MRD.

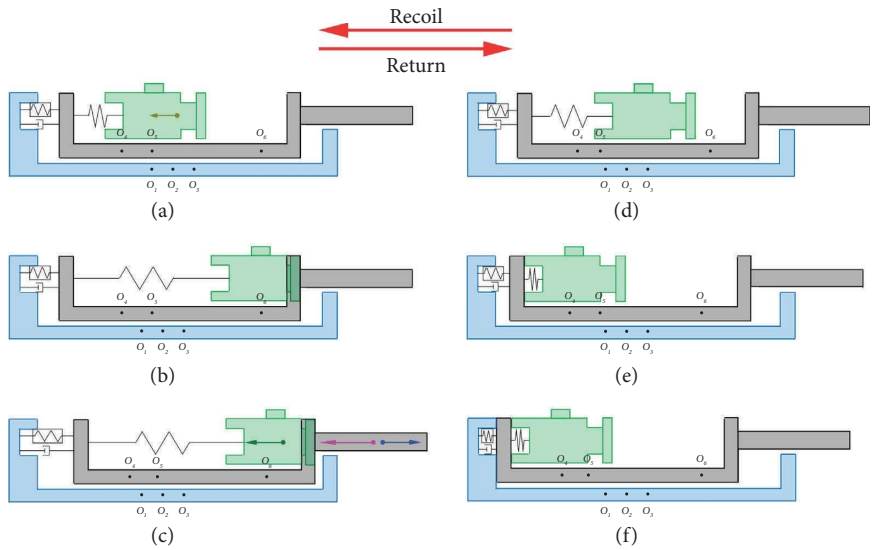

Figure 3: Schematic of the firing cycle of the floating machine gun.

receiver also slows because of the action of the bi-directional buffer spring. In Figure 3(e), the automaton has just recoiled to O_4, and has thus collided with the inner receiver, thereby propelling it to recoil further.

Figure 3(f) illustrates the maximum recoil positions attained by both the inner receiver and the automaton. The automaton then initiates its return motion, which is propelled by the reset spring, while the inner receiver decelerates

due to the action of the bi-directional buffer spring. Ultimately, the automaton and inner receiver return to their initial states depicted in Figure 3(a).

After establishing the three-dimensional structural assembly model of the floating machine gun on the UG CAD platform, the model is imported into the Adams mechanical simulation software. Motion joints and contact relationships between gun parts are defined within the software. The motion joint between the automaton and the inner receiver is a translational joint; they are connected by the reset spring, and contact-impact effects occur when the recoil and return are in place. The motion joint between the receiver and the inner receiver is also a translational joint, connected by the bi-direction buffer spring. Contact-impact effects occur between the inner receiver and the receiver when the recoil is in place. By fixing the receiver and applying the same motion relationships between other components as in reality and handling contact-impact constraints while applying the main loads, a simulation model of the floating machine gun with the same motion principles as shown in Figure 4 can be obtained. The relevant model parameters are listed in Table 1.

2.2. Determination of the Main Load. As shown by the purple, blue, green, and yellow arrows in Figure 3, the model presented in this paper contains four forces. The internal ballistic pressure can be expressed by the following equation [13-14]:

$$\begin{cases} \psi = \chi Z\left(1 + \lambda Z + \mu Z^2\right), \\ \dfrac{\mathrm{d}Z}{\mathrm{d}t} = \dfrac{P}{I_k}, \\ \mathrm{Spdt} = \varphi m_i \mathrm{d}v, \\ \mathrm{Sp}\left(1 + l_\psi\right) = \mathrm{fm}_p\psi + \dfrac{\theta}{2}\varphi \mathrm{m}_i v^2, \\ v = \dfrac{\mathrm{d}l}{\mathrm{d}t_i}, \\ l_\psi = l_0\left(1 - \dfrac{\triangle}{\delta} - \triangle\left(\alpha - \dfrac{1}{\delta}\right)\psi\right). \end{cases} \tag{1}$$

In equation (1), t_i represents the interior ballistic time, l is the bullet displacement in the barrel, p is the gas pressure, v represents the bullet velocity, ψ is the mass percentage of the burned propellant, Z is the relative burned thickness of the propellant, S denotes the equivalent area of the barrel cross-section, and W_0 is the equivalent volume of the piston chamber. In addition, m_p represents the propellant mass, δ is the propellant density, m_i is the bullet mass, l_0 denotes the initial equivalent volume of the barrel, $\triangle$ is the propellant charge density, I_k is the impulse of the propellant gas pressure, α represents the residual volume of the propellant gas, f is the propellant force, φ is a coefficient, and p_0 denotes the extrusion pressure. Furthermore, χ, λ, and μ represent the features of the powder shape.

The after-effect period of the interior ballistic pressure can be mathematically expressed by the following equation:

$$\begin{cases} p_a = p_k e^{-\left(t_h/b\right)}, \\ b = \dfrac{(\beta - 0.5)\, m_p v_0}{S\left(p_k - p_e\right)}, \\ \beta = \dfrac{1110}{v_0}, \end{cases} \tag{2}$$

where p_a represents the after-effect period pressure, v_0 is the muzzle velocity, P_k is the mean muzzle pressure at the instant when the bullet traverses the muzzle, P_e is 1.8 times the atmospheric pressure, t_h denotes the duration time calculated from the moment the bullet exits the muzzle, and β is the after-effect coefficient.

The piston cylinder pressure can be calculated using Bravin's formula, as shown in the following equation:

$$\begin{cases} P_s = P_d e^{-\left(t'/c\right)} 1 - e^{-a\left(t'/c\right)}, \\ i_0 = \dfrac{P_d + P_k}{2}\, t_{\mathrm{dk}} + \dfrac{\beta - 0.5}{S}\, m_p v_0, \\ b = \dfrac{i_0}{p_d}. \end{cases} \tag{3}$$

In equation (3), P_s represents the piston cylinder pressure, P_d is the mean pressure within the barrel at the instant when the bullet traverses the gas port, t' is the duration time calculated from the moment the bullet exits the gas port, a is a structural coefficient, c is a time constant, and t_{dk} denotes the duration of the bullet travel from the gas port to the muzzle. Figure 5 illustrates the internal ballistic pressure and the piston cylinder pressure. The internal ballistic force and the piston cylinder force can be calculated by multiplying the corresponding pressures and effective areas, as shown in the following equation:

$$\begin{cases} F_i = \begin{cases} pS, & 0 \le t \le t', \\ p_a S, & t \ge t', \end{cases} \\ F_{\mathrm{ch}} = P_s S_s. \end{cases} \tag{4}$$

In equation (4), F_i represents the force exerted by the internal ballistic process, F_{ch} denotes the force exerted by the piston cylinder, and S_s is the effective area of the piston cylinder. To ensure accurate modeling of the dynamic behavior of the belt, a rigid-flexible coupling model was constructed using the MPC-BRE2 method [15]. Experimental measurements of the feeding resistance are presented in Figure 6.

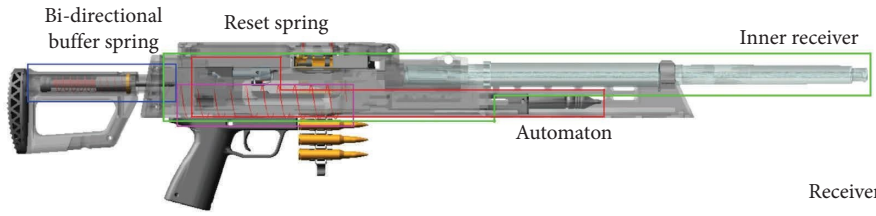

Figure 4: Dynamic simulation model of the floating machine gun.

Table 1: Parameters of the floating machine gun model.

Parameter	Energy storage (J)	Parameter	Mass (kg)	Parameter	Length (mm)
Bi-directional buffer spring	4.6	Automaton	1.33	Extreme recoil displacement	19.1
Reset spring	8	Inner receiver	5.6	Extreme return displacement	19.1

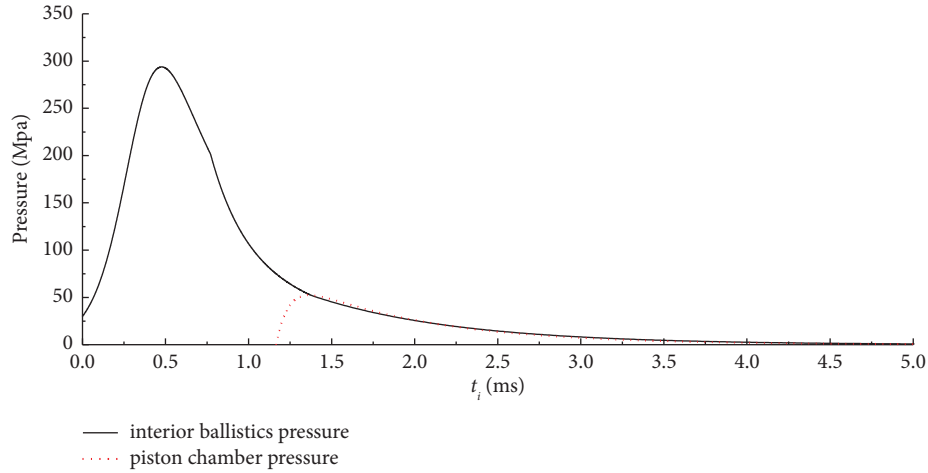

Figure 5: Pressure-time curves of the interior ballistic and piston cylinder pressures.

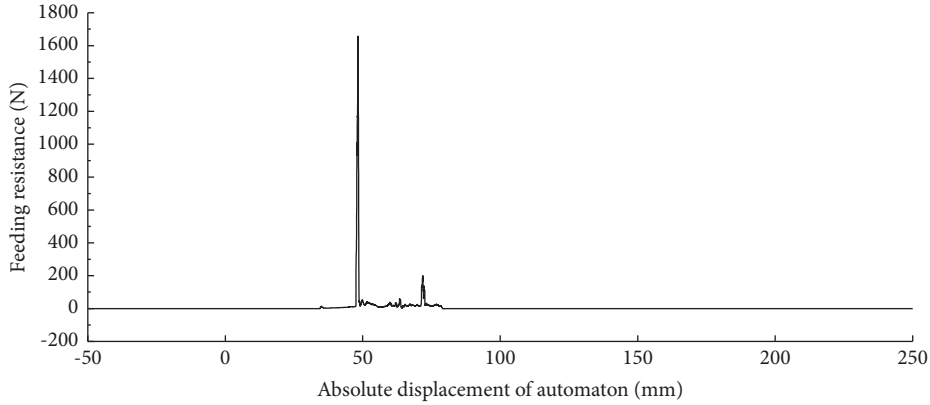

Figure 6: Feeding resistance as a function of the absolute displacement of the automaton.

3. Model Verification

The experiment takes place in an indoor firing range. The experimental system consists of a floating machine gun, a FASTCAM AX200 high-speed camera, and PCC 2.8 image processing software. The machine gun is mounted on a fixed stand, and markers are placed on the inner receiver and automaton. High-speed photography is used to capture the movement of firearm components. The experiment involves a 5-round burst with a frame rate of 5,000 frames per second.

The PCC 2.8 image processing software is then used to extract the positions and times of the markers in the captured videos, allowing the derivation of displacement-time curves for the inner receiver and automaton. Further data processing yields velocity-time curves.

Figures 7 and 8 depict comparisons between the experimentally and simulation automaton velocity-time curves and inner receiver displacement-time curves, respectively. Table 2 compiles statistics on factors such as firing rate, automaton maximum recoil speed, maximum return speed, MRD, and inner receiver maximum return displacement. In comparison with experimental results, the maximum error of the simulation model is 8.0%, confirming the accuracy of the simulation model. The close agreement between the simulation and experimental results demonstrates the accuracy of the simulation model.

Figure 7 shows that the firing rate of the firearm was 367.3 rounds/min. Figure 8 depicts the displacement-time curves for the inner receiver, which can also be understood as the vibration of the inner receiver. An MRD value of 19.1 mm was obtained.

It is noteworthy that a certain degree of error was present in both the experimental and simulation curves. In the simulation model, an equivalent feeding resistance of the belt chain was determined using flexible bodies, and the piston cylinder and internal ballistic pressures were calculated using empirical formulas, which resulted in constant force values.

In reality, variations existed in the individual belt-chain conditions, and the feeding resistance was not the same for each round of ammunition. The combustion conditions of the gunpowder were also not identical for each round of ammunition, which caused variations in the gas pressure and internal ballistic forces. Furthermore, the locking, extraction, and ejection process of the firearm all involved subtle material deformations, which were simplified for the simulation model. Hence, there was a certain degree of error between the simulation and experimental results.

4. Combination Optimization Design

The physical prototype manufacturing process of firearms is exceedingly lengthy, often requiring one to two years. In addition, some experiments pose dangers, and conducting parameter variation tests is challenging and costly. As a novel principle machine gun, the presence of inner receiver makes the floating firearm a typical dual-degree-of-freedom system. Moreover, within the system, there are numerous impact and momentum transfer processes, leading to a plethora of potential influencing factors. The coupling effects of multiple parameters are highly complex and peculiar, given that most of these factors have not been previously studied, and their impact levels remain unknown. This presents numerous challenges in achieving a rational parameter matching design for current floating machine guns. The challenge is addressed by employing the Combination Optimization Design method in this paper.

In this study, a comprehensive optimization design approach was developed to enhance the performance of the floating machine gun. This approach accounted for the effects of multiple factors. A schematic representation of the design process is depicted in Figure 9. The initial step involved selecting the influential factors for the orthogonal design; the MRD and the firing rate were chosen as the evaluation criteria. Subsequently, the simulation model, which was discussed in Section 2, was used to assess the performance of the floating machine gun under various combinations of factors.

The SPSS software is used to conduct analyses of variance and generate F values. The F value serves as an indicator for assessing the degree of parameter impact, where a larger F value indicates a more significant influence. The statistical significance level is a conversion index for the F value, used to evaluate the meaningfulness of the results. It is generally considered that when the statistical significance level is less than 0.1, the impact is considered meaningful. Finally, the optimal levels of the highly significant factors were identified for integration, resulting in an optimized combination scheme [16, 17].

4.1. Factor Selection and Orthogonal Design. Factors that commonly influence traditional firearm operation, such as the automaton mass, the reset spring energy storage, and the piston cylinder pressure, as well as factors specific to the floating machine gun, such as the inner receiver mass, the bidirectional buffer spring energy storage, the internal ballistic pressure, and the reset spring position, were used as factors in the orthogonal design [18–20]. The reset spring position was assigned two levels, A1 and A2, which indicate inner receiver-automaton and receiver-automaton positions, respectively. Three levels were chosen to represent the states of the remaining factors: minimum, medium, and maximum. The specific parameter values are summarized in Table 3, while the orthogonal scheme is presented in Table 4. Due to practical engineering considerations, the variation ranges were not uniform for factors B through G.

The selection of factors and levels in this paper is primarily based on design rules and engineering experience. For example, the choice of reset spring position is based on different designers' perspectives. Similarly, internal ballistic pressure is a common variable in firearm design, but it directly determines the velocity and power of the bullet, and its range of variation is very limited. A common engineering variation range is from 0.9 times to 1.1 times.

4.2. Analysis of Simulation Results. The results of the variance analysis are presented in Figures 10 and 11. Equation (5) presents the variance analysis calculation process [21, 22]:

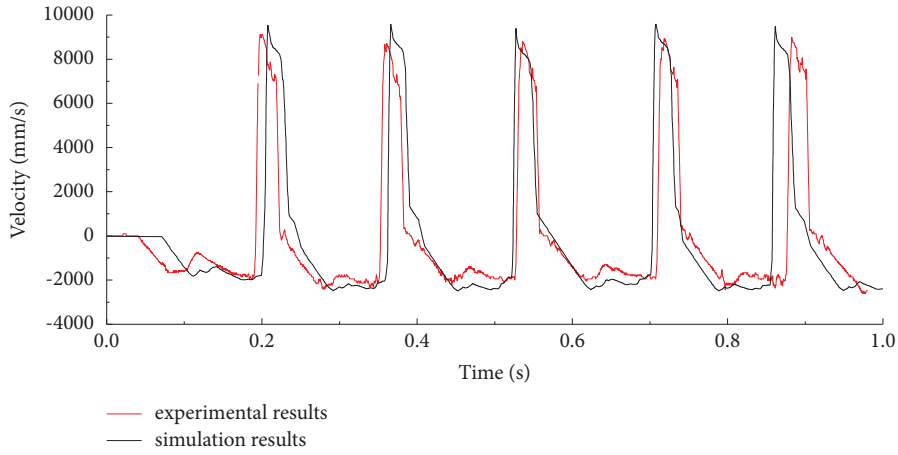

Figure 7: Automaton velocity-time curves.

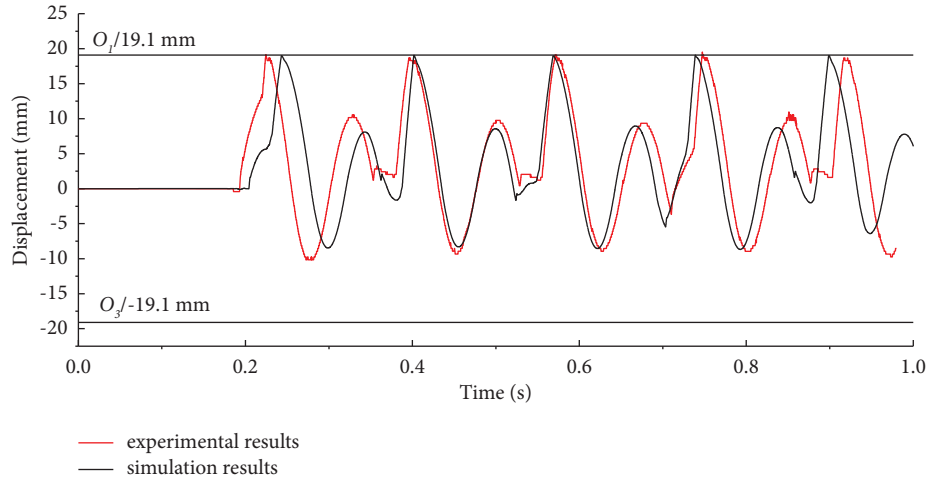

Figure 8: Inner receiver displacement-time curves.

Table 2: Variation ranges of various factors.

	Firing rate (rounds/min)	Automaton maximum recoil speed (mm/s)	Automaton maximum return speed (mm/s)	MRD (mm)	Inner receiver maximum return displacement (mm)
Experimental results	367.3	9153.6	−2267.8	19.1	−9.4
Simulation results	367.2	9114.7	−2464.6	19.1	−8.8
Error (%)	0.1	0.4	8.0	0	6.8

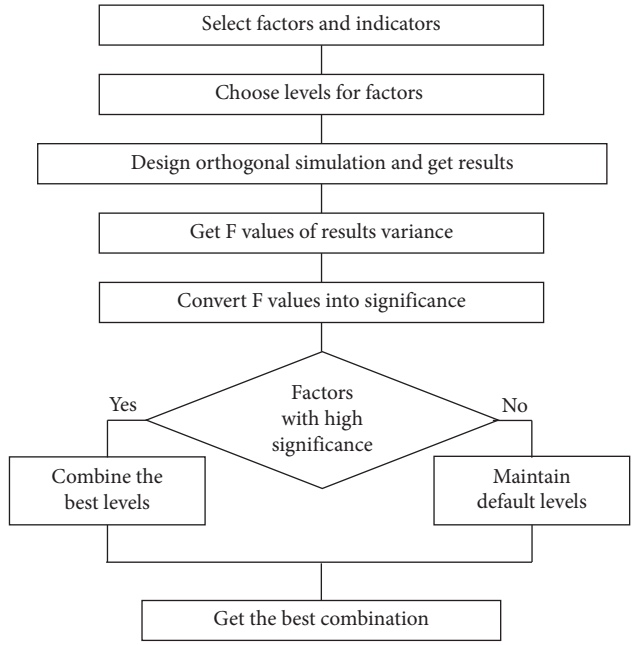

Figure 9: Combined optimization design process.

$$\begin{cases} \overline{x_i} = \dfrac{\sum_{j=1}^{n_i} x_{ij}}{n_i}, \\ \bar{\bar{x}} = \dfrac{\sum_{i=1}^{k}\sum_{j=1}^{n_i} x_{ij}}{n}, \\ \mathrm{MSA} = \dfrac{\sum_{i=1}^{k} n_i\left(\overline{x_i} - \bar{\bar{x}}\right)^2}{k-1}, \\ \mathrm{MSE} = \dfrac{\sum_{i=1}^{k}\sum_{j=1}^{n_i}\left(x_{ij} - \overline{x_i}\right)^2}{n-k}, \\ F = \dfrac{\mathrm{MSA}}{\mathrm{MSE}}, \end{cases} \tag{5}$$

where n represents the total number of tests, x_{ij} is the result value for the i^{th} level of the j^{th} factor, $\overline{x_i}$ denotes the mean value of level i, n_i and k represent the total number of factors and maximum number of levels, respectively, and $\bar{\bar{x}}$ is the mean value of all 18 test results.

With regards to the MRD indicators, the F values corresponding to parameters A, B, C, D, E, F, and G were determined to be 1.9, 2.467, 8.069, 12.139, 1.921, 6.394, and 2.289, respectively. After conversion, the statistical significance level of the piston cylinder pressure (C) was determined to be 0.039. In addition, the significance level of the bi-directional buffer spring energy storage (D) was found to be 0.02, while the significance level of the inner receiver mass (F) was determined to be 0.057. For all these cases, the significance levels were determined to be less than 0.1.

The mechanism by which piston cylinder pressure (C), energy storage of the bi-directional buffer spring (D), and inner receiver mass (F) influence MRD is as follows: for a single-degree-of-freedom system composed of the inner receiver and bi-directional buffer spring, piston cylinder pressure (C) serves as the excitation to the system. The energy storage of the bi-directional buffer spring (D) and inner receiver mass (F) act as the equivalent spring stiffness and mass of the system, directly affecting the inherent amplitude and frequency of the single-degree-of-freedom system. Although the actual amplitude is highly influenced by impacts between the automaton and inner receiver, the inherent amplitude and frequency also have a significant impact on MRD.

These significance levels indicate that three parameters most significantly affect the MRD. Notably, the MRD is minimized when the piston cylinder pressure is at its minimum level (C1), the bi-directional buffer spring energy storage is at its maximum level (D3), and the inner receiver mass is at its medium level (F2).

With regards to the firing rate indicator, the F values corresponding to parameters A, B, C, D, E, F, and G were determined to be 2.131, 3.959, 1.7, 0.852, 35.888, 0.753, and 79.756, respectively. After conversion, the significance level of the automaton mass (G) was determined to be 0.003, while the significance level of the reset spring energy storage (E) was found to be 0.001. For both cases, the significance levels were determined to be less than 0.1.

The factors affecting firing rate, reset spring energy storage (E), and automaton mass (G) are explained as follows: the reset spring is responsible for propelling the automaton to complete the return motion. Therefore, a larger reset spring energy storage (E) and a smaller automaton

Table 3: Variation ranges of various factors.

State	Internal ballistic pressure	Piston cylinder pressure	Energy storage of the bi-directional buffer spring (J)	Energy storage of the reset spring (J)	Inner receiver mass (kg)	Automaton mass (kg)
	B	C	D	E	F	G
Minimum	0.9 × initial interior ballistic pressure	0.8 × initial piston cylinder pressure	2.3	6.4	3.92	0.93
Medium	Initial interior ballistic pressure	Initial piston cylinder pressure	4.6	8	5.6	1.33
Maximum	1.1 × initial interior ballistic pressure	1.2 × initial piston cylinder pressure	6.9	9.6	7.28	1.73

Table 4: Orthogonal scheme.

Trial	Level combination	Trial status description						
1	A1B1C1D1E1F1G1	Inner receiver-automaton	Min	Min	Min	Min	Min	Min
2	A1B1C1D3E2F2G2	Inner receiver-automaton	Min	Min	Max	Med	Med	Med
3	A1B1C2D2E2F2G3	Inner receiver-automaton	Min	Med	Med	Med	Med	Max
4	A1B1C3D2E3F1G1	Inner receiver-automaton	Min	Max	Med	Max	Min	Min
5	A1B2C1D2E1F3G3	Inner receiver-automaton	Med	Min	Med	Min	Max	Max
6	A1B2C2D1E2F3G1	Inner receiver-automaton	Med	Med	Min	Med	Max	Min
7	A1B2C2D3E1F1G2	Inner receiver-automaton	Med	Med	Max	Min	Min	Med
8	A1B2C3D1E3F2G3	Inner receiver-automaton	Med	Max	Min	Max	Med	Max
9	A1B3C1D2E3F3G2	Inner receiver-automaton	Max	Min	Med	Max	Max	Med
10	A1B3C2D3E3F1G3	Inner receiver-automaton	Max	Med	Max	Max	Min	Max
11	A1B3C3D1E1F2G2	Inner receiver-automaton	Max	Max	Min	Min	Med	Med
12	A1B3C3D3E2F3G1	Inner receiver-automaton	Max	Max	Max	Med	Max	Min
13	A2B1C2D1E3F3G2	Receiver-automaton	min	Med	Min	Max	Max	Med
14	A2B1C3D3E1F3G3	Receiver-automaton	min	Max	Max	Min	Max	Max
15	A2B2C1D3E3F2G1	Receiver-automaton	Med	Min	Max	Max	Med	Min
16	A2B2C3D2E2F1G2	Receiver-automaton	Med	Max	Med	Med	min	Med
17	A2B3C1D1E2F1G3	Receiver-automaton	Max	min	min	Med	Min	Max
18	A2B3C2D2E1F2G1	Receiver-automaton	Max	Med	Med	Min	Med	Min

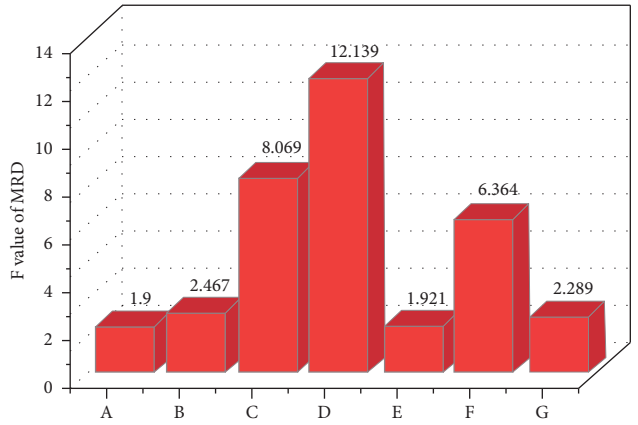

Figure 10: F values of the seven parameters that influence the MRD.

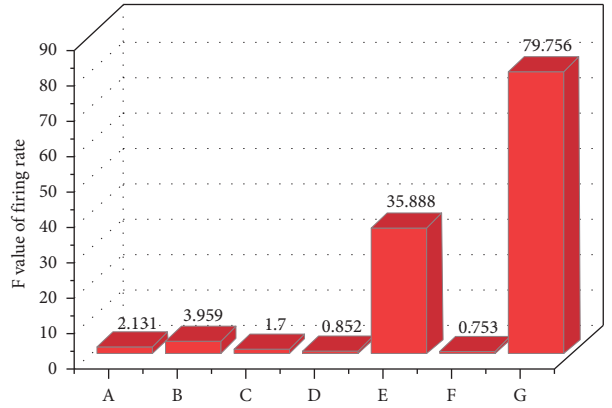

Figure 11: F values of the seven parameters that influence the firing rate.

Table 5: Comparison between the optimal combination results and the experimental results.

Results	MRD (mm)	Firing rate (rounds/min)
Initial test	19.1	367.3
Final optimal combination	15.24	465

mass (G) result in a faster return motion of the automaton, leading to a higher firing rate of the firearm.

It was therefore concluded that the firing rate is primarily influenced by the automaton mass and the energy storage of the reset spring. Notably, the firing rate is maximized when the reset spring energy storage is at its maximum level (E3) and the automaton mass is at its minimum level (G1).

4.3. Comparison of Results. To enhance the performance of the floating machine gun designed during this study, reducing the MRD was a crucial objective. The C1D3F2 combination was selected as the preliminary optimal configuration. However, during the initial test, an unacceptably low firing rate of 367.3 rounds per minute was obtained. To improve the firing rate, the E3G1 combination was identified as the optimal configuration. The remaining factors were maintained at their default settings of A1B2. Consequently, the final optimal combination was determined to be A1B2C1D3E3F2G1. Table 5 compares the results for the final optimal combination with the initial test data.

Using the optimized parameter combination for the firearm resulted in an MRD reduction from 19.1 mm to 15.24 mm and an increase in the firing rate from 367.3 rounds/min to 465 rounds/min. These values represent a 20.2% reduction in the MRD and a 26.6% increase in the firing rate from the values produced by the initial combination.

For a floating machine gun, designers often ensure sufficient space redundancy to achieve floating successfully. Unsuccessful floating can be detrimental to the firearm's shooting accuracy and imposes significant spatial and structural constraints, affecting reliability and adding weight. Therefore, reducing the MRD is advantageous for improving reliability, reducing weight, and effectively enhancing the firearm's floating performance. In addition, floating machine guns often have lower firing rates, resulting in lower firepower density, which is unacceptable for machine guns. In practical engineering applications, the common issue in floating machine gun design is the synchronous occurrence of larger MRD and lower firing rates. Therefore, the ability to simultaneously reduce MRD and increase firing rates significantly improves the firearm's performance.

5. Conclusions

In this study, a two-degree-of-freedom simulation model was developed for a floating machine gun. The simulation results agreed well with experimental observations, accurately depicting the motion characteristics of the inner receiver and the automaton. By combining experimental and orthogonal simulation methods, a thorough examination of the effects of seven parameters on the floating performance was conducted.

A combination optimization revealed that the piston cylinder pressure, the bi-directional buffer spring energy storage, and the inner receiver mass all significantly affect the MRD. In contrast, the energy storage of the reset spring and the automaton mass notably affect the firing rate. The other parameters investigated do not exhibit obvious correlations with the floating machine gun performance.

The optimal combination of parameter values was determined by applying an optimization approach. It included a reset spring placement between the inner receiver and the automaton, a medium interior ballistic pressure, a small piston cylinder pressure, large bi-directional buffer spring and reset spring energy storage values, a medium inner receiver mass, and a small automaton mass. This optimized combination resulted in a remarkable MRD reduction of approximately 20.2% and a substantial firing rate increase of approximately 26.6%; these improvements effectively enhanced the overall performance of the floating machine gun. Similar methods can be applied to address other performance aspects of floating machine guns or similar engineering problems.

Data Availability

The data used to support the findings of this study are included within the article.

Disclosure

This manuscript was previously published on Research Square as a preprint, and the URL is https://www.researchsquare.com/article/rs-2081879/v1. This version of the manuscript represents the latest improvements, and in the references section, I have also included the Research Square preprint as a citation.

Conflicts of Interest

The authors declare that they have no conflicts of interest.

Authors' Contributions

This research article involved the contributions of Yang Wang, Cheng Xu, Long He, and Yanfeng Cao. Yang Wang was primarily responsible for the initial drafting of the manuscript and the experimental design, while Cheng Xu provided review and research supervision. Long He and Yanfeng Cao participated in the experimental work. Additionally, Yanfeng Cao was responsible for the manuscript's revision and correction. All authors have thoroughly reviewed and approved the final version of the manuscript, agreeing to its publication.

Acknowledgments

This research was supported by the National Natural Science Foundation of China (Grant no. 52275256).

References

[1] Y. P. Wang, *Gun and Automatic Weapon Dynamics*, Beijing University of Technology Press, Beijing, China, 2014.

[2] D. Steimke, G. Rossier, L. Hayes, and D. Parker, "Short recoil impulse averaging weapon system," 2014, https://patents.google.com/patent/US20130047833A1/en.

[3] D. Luke Steimke, J. John Melochick, A. Phillip Loriot, J. Thomas Shawley, and L. Lee Bunch, "Recoil assembly for a machine gun," 2023, https://patents.google.com/patent/US20190331450A1/en.

[4] Z. T. Fan, "Performance of a floating mechanism with a fixed constraint and secondary recoil," *Journal of Vibration and Shock*, vol. 34, no. 6, 2015.

[5] Z. C. Li and J. Wang, "A gun recoil system employing a magnetorheological fluid damper," *Smart Materials and Structures*, vol. 21, no. 10, Article ID 105003, 2012.

[6] Y. Lu, K.-D. Zhou, L. He, J.-S. Li, and X.-Y. Huang, "Research on the floating performance of a novel large caliber machine gun based on the floating principle with complicated boundary conditions," *Defence Technology*, vol. 15, no. 4, pp. 607–614, 2019.

[7] Y. Lu, K. Zhou, H. Lei, J. Li, and X. Huang, "Research on influence of muzzle brake efficiency on a new large caliber machine gun based on floating principle," *Acta Armamentarii*, vol. 37, no. 9, p. 1585, 2016.

[8] J. S. O. N. G. Jie, L. I. A. O. Zhen-qiang, L. I. Jia-sheng, and X. I. A. O. Jun-bo, "Dynamics characteristics of automatic mechanism for gas operated and floating barrel operated automatic action," *Acta Armamentarii*, vol. 35, no. 6, p. 753, 2014.

[9] J. Song, P. Si, Z. Liao, and M. Qiu, "Launch dynamics analysis of a grenade machine gun with high muzzle velocity based on the soft recoil technology," *Journal of Physics: Conference Series*, vol. 2459, no. 1, Article ID 12102, 2023.

[10] Y. Wang, *Research on Structural Scheme and Dynamic Characteristics of a Medium Caliber Machine Gun*, Nanjing University of Science and Technology, Nanjing, China, 2017.

[11] L. Yongjian, W. Shan, A. Jie, and Z. Junnuo, "Research on low recoil launch technology of small UAV with small arms mounted on it based on floating principle," *Journal of Physics: Conference Series*, vol. 1314, no. 1, Article ID 12081, 2019.

[12] D. Ning, S. Sun, H. Du, W. Li, and W. Li, "Control of a multiple-DOF vehicle seat suspension with roll and vertical vibration," *Journal of Sound and Vibration*, vol. 435, pp. 170–191, 2018.

[13] Z. M. Jin, *Interior Ballistics of Gun*, Beijing Institute of Technology Press, Beijing, China, 2004.

[14] Q. Sun, G. Yang, and J. Ge, "Modeling and simulation on engraving process of projectile rotating band under different charge cases," *Journal of Vibration and Control*, vol. 23, no. 6, pp. 1044–1054, 2017.

[15] B.-J. Zhang, R.-L. Wang, L. I. Yong-jian, and C. Han, "Modeling and analysis of the release process of open projectile chain," *Acta Armamentarii*, vol. 32, no. 12, pp. 1531–1534, 2011.

[16] Y. Wang, Y.-P. Wang, and C. Xu, "Experimental study: effects of typical man-rifle parameters on aiming performance," *Journal of Physics: Conference Series*, vol. 1507, no. 10, Article ID 102012, 2020.

[17] C. L. Kuo, C. K. Yuan, B. S. Liu, and B.-S. Liu, "Using human-centered design to improve the assault rifle," *Applied Ergonomics*, vol. 43, no. 6, pp. 1002–1007, 2012.

[18] T. D. Vu, S. Procházka, Z. Krist, and B. V. Vo, "Influence of gas port on forces and their impulses acting in an automatic weapon," in *Proceedings of the 2021 International Conference on Military Technologies (ICMT)*, IEEE, Brno, Czech Republic, June 2021.

[19] S. Li, L. Qiang, Q. Tan, and C. Ma, "Optimization design of certain type gatling gun weapon buffer spring device based on isight," *Ordnance Industry Automation*, vol. 37, no. 5, pp. 49–51+59, 2018.

[20] C. Ma, L. Qiang, and C. Cheng, "Parameter design of certain type gatling gun buffer device based on ADAMS," *Ordnance Industry Automation*, vol. 35, no. 11, pp. 32–36, 2016.

[21] R. Liu, Y. Zhang, C. Wen, and J. Tang, "Study on orthogonal experimental design and analysis method," *Experimental Technology and Management*, vol. 27, no. 9, pp. 52–55, 2010.

[22] Y. Wang, C. Xu, and L. He, "A multi factor combination optimization design of a two degree of freedom mechanical system," 2022, https://assets.researchsquare.com/files/rs-2081879/v1/1699c6fb-8a40-409e-94e4-68129bd028e0.pdf?c=1667456079.